SYNTHESIS AND APPLICATION OF MXENE ($Ti_3C_2t_X$) IN ELECTROCHROMISM

M.Sc. Thesis

By

DIVYANSH MISHRA

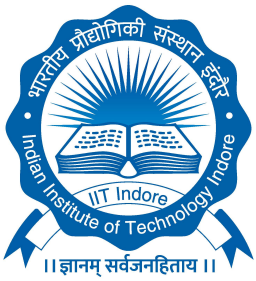

DEPARTMENT OF PHYSICS

INDIAN INSTITUTE OF TECHNOLOGY INDORE

MAY 2025

SYNTHESIS AND APPLICATION OF MXENE ($Ti_3C_2t_X$) IN ELECTROCHROMISM

A THESIS

Submitted in partial fulfillment of the requirements for the award of the degree

of
Master of Science

by
DIVYANSH MISHRA

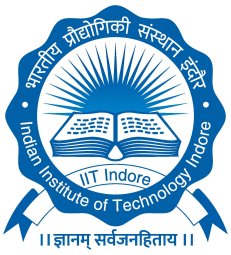

DEPARTMENT OF PHYSICS
INDIAN INSTITUTE OF TECHNOLOGY INDORE
May 2025

INDIAN INSTITUTE OF TECHNOLOGY INDORE

CANDIDATE'S DECLARATION

I hereby certify that the work which is being presented in the thesis entitled **Synthesis and Application of MXene ($Ti_3C_2t_x$) in Electrochromism** in the partial fulfillment of the requirements for the award of the degree of **MASTER OF SCIENCE** and submitted in the **DEPARTMENT OF PHYSICS**, Indian Institute of Technology Indore, is an authentic record of my own work carried out during the time period from **July 2024** to **May 2025** under the supervision of **Prof. Rajesh Kumar, Professor, Department of Physics, IIT Indore**.

The matter presented in this thesis has not been submitted by me for the award of any other degree of this or any other institute.

Signature of the student with date
(DIVYANSH MISHRA)

.....

This is to certify that the above statement made by the candidate is correct to the best of my knowledge.

Signature of the Supervisor
(Prof. Rajesh Kumar)

.....

Divyansh Mishra has successfully given his M.Sc. Oral Examination held on **May 14, 2025**.

Signature of Supervisor of M.Sc. thesis
Date: 21/05/2025

Signature of Convener, DPGC
Date: 25/06/2025

ACKNOWLEDGMENT

First and foremost, I thank my supervisior, **Prof. Rajesh Kumar**, for their invaluable guidance, encouragement, and expertise. His insightful support has been instrumental not only in shaping the direction of my research but also in contributing to my personal and professional growth.

I would also like to extend my sincere gratitude to my secondary school physics teacher, **Mr. Bhupendra S. Bhadouria**, for sparking my interest in the field of physics and for his unwavering encouragement towards the pursuit of my aspirations, both academic and personal.

I also extend my appreciation to my research mentor and colleagues for their collaboration and support. Their mentorship made the research process enjoyable and productive. I am grateful to **Indian Institue of Technology Indore** and **MAD Lab** for providing the necessary resources and facilities to conduct my experiments.

Finally, I would like to acknowledge my family and friends for their unwavering support and encouragement. Their belief in me has been a constant source of motivation.

I sincerely thank everyone who has contributed to this work in any capacity.

DIVYANSH MISHRA
Master of Science

Abstract

Two-dimensional (2D) materials are increasingly vital in advancing compact and efficient technologies. MXenes, a novel class of 2D materials, offer promising electrical and electrochemical properties, yet their potential in electrochromic applications remains underexplored. This study investigates the effect of $Ti_3C_2t_x$ MXene doping on electrochromic device performance, focusing on switching behaviour, stability, and charge dynamics. MXene was synthesised via two methods: direct etching of MAX phase using hydrofluoric acid, and an in situ approach involving lithium fluoride and hydrochloric acid. The resulting materials were characterised and validated against a reference MXene sample. For electrochromic evaluation, $V_2O_2(OH)_3$, a vanadium-based complex with promising charge storage capabilities, was selected, with polyaniline (PANI) assessed for compatibility. Devices fabricated with these materials were evaluated using UV-Vis spectroscopy and electrochemical methods. While the undoped device exhibited high optical contrast, its switching speed and stability were limited. MXene doping resulted in faster switching and improved stability, though accompanied by a modest reduction in colour contrast due to the dopant's dark appearance. Enhanced colouration efficiency indicated better ion transport and electrochemical response, demonstrating the potential of MXene to improve multifunctional electrochromic systems.

Contents

List of Figures

List of Tables

Chapter 1

Introduction

The discovery of Graphene opened up a new path for exploring a class of materials known as "Two Dimensional (2-D) materials". Driven by the success of graphene, alternative layered and non-layered 2-D materials have gained significant research attention due to their unique physical and chemical properties. The origin of these properties is attributed to the effects of dimensionality and the modulation of their band structure [1].

Two-dimensional materials, generally consisting of just one or two atoms in thickness, possess unique properties that distinguish them from bulk materials. Some of the properties are as follows:

Mechanical properties : 2-D materials possess higher strength as compared to Three Dimensional (3-D) materials because they have a larger surface area relative to their volume. 2-D materials are known for their excellent mechanical properties, such as high strength and stiffness, even though they are very thin [2].

Optical properties : 2-D materials present unique opportunities that traditional semiconductors cannot provide. As research progresses, the ability to tune their optical properties through external modulation techniques shows great potential for developing high-performance optoelectronic devices [3].

Electronic properties : The electronic properties of 2-D materials, including high carrier mobility, adjustable band gaps, and spin-orbit coupling, are particularly remarkable. These features create potential for advancements in nano-electronics, flexible devices, and optoelectronic applications [4].

Since the discovery of graphene, many 2-D materials have been studied, each offering unique properties and potential uses. These materials include transition metal dichalcogenides (TMDs), black phosphorus (BP), hexagonal boron nitride (h-BN), silicene, germanene, stanene, and various 2-D organic compound.

MXene is a relatively newly explored 2-D material. In this study, we will examine the various synthesis methods and explore the potential applications of MXene.

1.1 MXene: A newly explored 2-D material

MXenes are a unique type of 2-D material that has gained a lot of attention in recent years because of their special properties and many possible uses. They were first discovered in 2011 [5]. MXenes are made from transition metal carbides, nitrides, or carbonitrides and are known for their layered structure and complex surface chemistry.

The general formula for MXenes is $\mathbf{M}_{n+1}\mathbf{X}_n\mathbf{t}_x$ where M represents a transition metal, X is carbon or nitrogen, and t_x represents the surface terminals of MXene, such as -O, -OH, -F, -Cl, etc [6]. The discovery of MXenes has broadened the range of 2-D materials, adding examples such as $Ti_3C_2t_x$, Ti_2Ct_x, V_2C and $Ta_4C_3t_x$, etc [7]. The diverse chemical composition and distinctive layered structure of MXenes give them outstanding properties, including high metallic conductivity [8], exceptional optical characteristics [9], and strong mechanical properties [10], etc.

Recent advancements in the emerging field of MXenes have led to their exploration in various applications, including batteries [11], supercapacitors [11], catalytic application [12], and solar cells [13], optoelectronic devices, electro-magnetic interference shielding, and sensor applications [14], among others.

In this study, we have investigated the potential application of MXene in electrochromic devices. Although MXene is inherently black in color and lacks electrochromic properties, its use as a dopant in electrochromic materials can significantly enhance the performance and functionality of

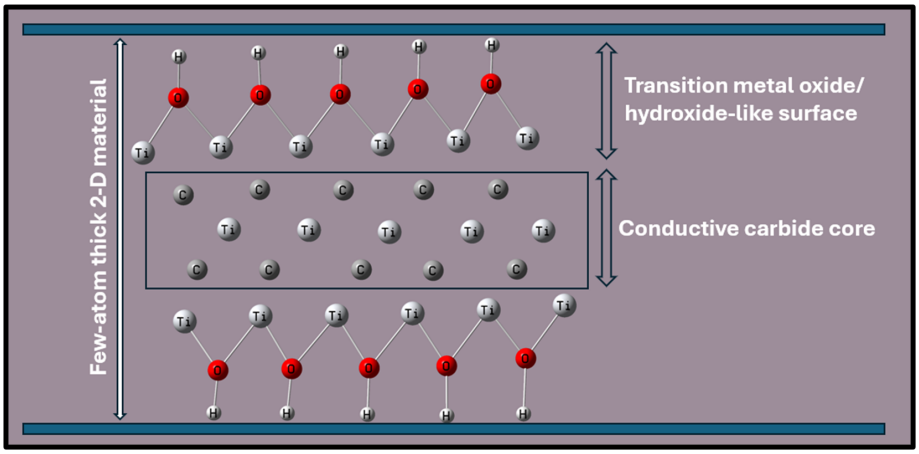

Figure 1.1: Chemical structure of MXene, i.e., $Ti_3C_2t_x$.

the device, thereby contributing to the development of a multifunctional electrochromic system.

MXenes are derived from the selective etching of MAX phase materials. MXenes were unexpectedly discovered during research on MAX phase materials for energy storage applications, revealing a new and exciting possibility. To better understand MXenes, it is important to first explore the properties and characteristics of MAX phase materials.

1.2 MAX phase materials

MAX phase materials serve as the parent materials for MXenes. Similar to MXenes, they also exhibit a range of unique properties. MAX phase is a nanolayered ternary compound characterized by a hexagonal lattice structure.

In 2000, Barsoum [15] provided a comprehensive description of this class of ceramic materials and introduced the concept of the "MAX phase" for the first time. In the $M_{n+1}AX_n$ phase (where n = 1, 2, 3), "M" denotes a transition metal element, "A" represents an A-group element, and "X" refers to either carbon or nitrogen. The positions of the elements M, A, and X in the periodic table are key to understanding the structure of the $M_{n+1}AX_n$ phase material. The MAX phase consists of alternating layers of MX sheets and A atoms arranged in a stacking sequence along the c-axis, Refer to Figure 1.2. Each layer of X atoms is positioned between two layers of transition metals, with every two layers of $M_{n+1}X_n$ separated by a single layer of A atoms [16].

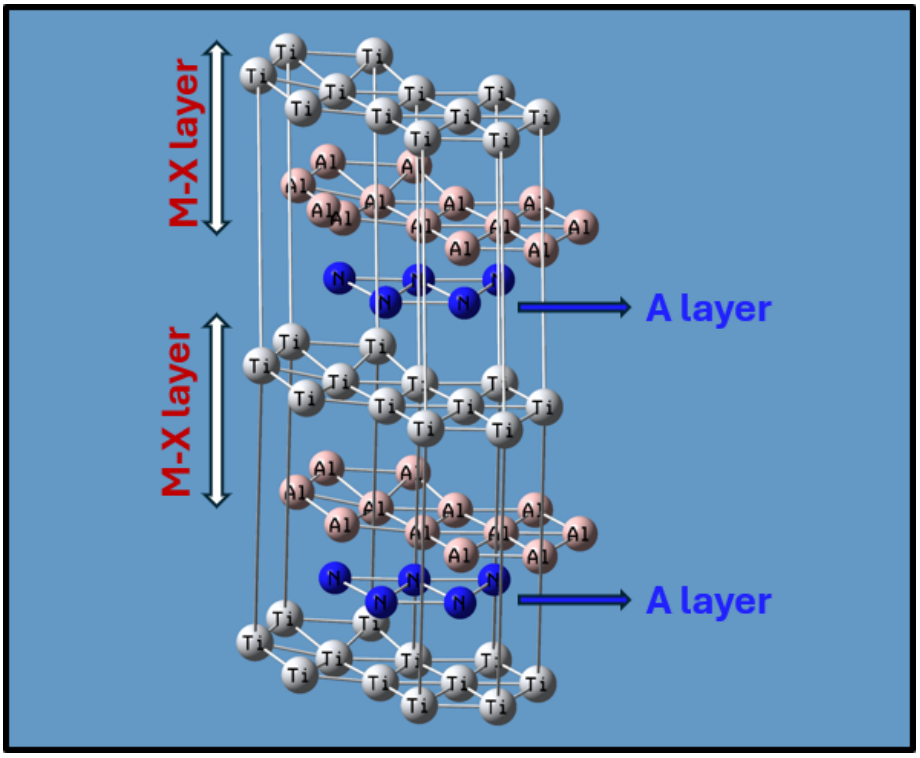

Figure 1.2: Chemical structure of MAX phase material, i.e., Ti_3AlC_2.

The electronic structure of the MAX phase shows that the M-X bond is strong, made up of both covalent and ionic bonds, while the M-A bond is weaker, involving covalent and metallic bonds. The M-M bond is a metallic bond, and the connection between the MX layer and the A atom layer is weak, making it easier for the A atoms to break away from the MX layer.

The presence of metallic bonds in MAX phase materials provides metallic properties such as high electrical conductivity, high thermal conductivity, and excellent damage tolerance. Additionally, the combination of covalent and ionic bonds in these materials gives them ceramic characteristics, including corrosion resistance, lightweight, and high elastic modulus. As a result, MAX phase materials exhibit a unique blend of both metallic and ceramic properties [17].

Due to its unique properties, MAX phase has a wide range of applications in areas such as high-temperature structural materials, high-temperature coatings, nuclear technology, catalysis, and as precursors for MXenes [17].

1.3 Electrochromism

Electrochromism is the phenomenon of optical modulation driven by an external electrical bias, and materials exhibiting this property are referred to as Electrochromic Materials (ECMs). The term "Electrochromism" was introduced by Platt in 1961 [18], following his discovery that a material can display different colors when subjected to varying bias conditions.

1.3.1 Elechtrochromic Materials (ECMs)

ECMs can generally be classified into three categories on the basis of applied potential. Categories are as follows:

Anodic or p-type ECMs: The material which changes its color when a positive bias is applied. For example, Poly(3-hexylthiophene)[P3HT].

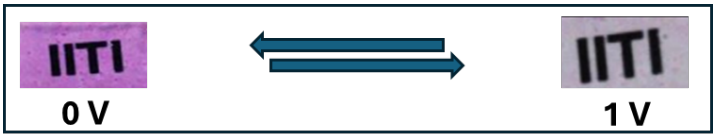

Figure 1.3: Optical modulation of P3HT electrode under positive bias.

Cathodic or n-type ECMs: The material which changes its color when a negative bias is applied. For example, Ethyl viologen diperchlorate [EV].

Figure 1.4: Optical modulation of EV electrode under negative bias.

Bipolar ECMs: The material which changes its color under both negative and positive biases. For example, Polyaniline [PANI]. [19]

Figure 1.5: Optical modulation of PANI electrode under positive and negative biases.

Electrochromism is observed because of the way material absorbs light in the visible range changes, when the material switches between different oxidation states. [20].

There are several applications related to the phenomenon of electrochromism. One of the most explored and widely used applications is electrochromic smart windows [19]. Smart windows are commonly used in planes and homes to control light intensity. Electrochromic goggles are another newly explored area related to this phenomenon. These goggles let you adjust the tint to control light and temperature, reducing glare and providing eye comfort in different environments [21].

Devices made from these materials that utilize this phenomenon are known as electrochromic devices (ECD) [19].

1.3.2 Electrochromic Devices (ECDs)

Devices that demonstrate electrochromism are known as electrochromic devices. On the basis of layers of electrochromic or non-electrochromic materials used to fabricate a device, we can categorise ECDs in three main categories:

Monolayer ECDs : A single electrochromic layer, combined with a blank electrode and an appropriate solid-state electrolyte, can be used to create a fully functional ECD. While its functionality may be limited, it is capable of displaying a color change in response to an external bias [22].

Bi-Layer ECDs : The bi-layer structure is considered the most reliable ECD design for practical applications. In this configuration, layers of are deposited separately onto two distinct substrates and then connected with an electrolytic gel placed in between. One of the layers is typically made of , while the other, which may or may not be , serves as the counter ion to facilitate the redox process of the electrochromic layer [22].

Composite ECDs : These types of ECDs are commonly constructed using composite films. When one material is deposited on top of another, it creates a core-shell structure, resulting films are more durable and exhibit enhanced stability [22].

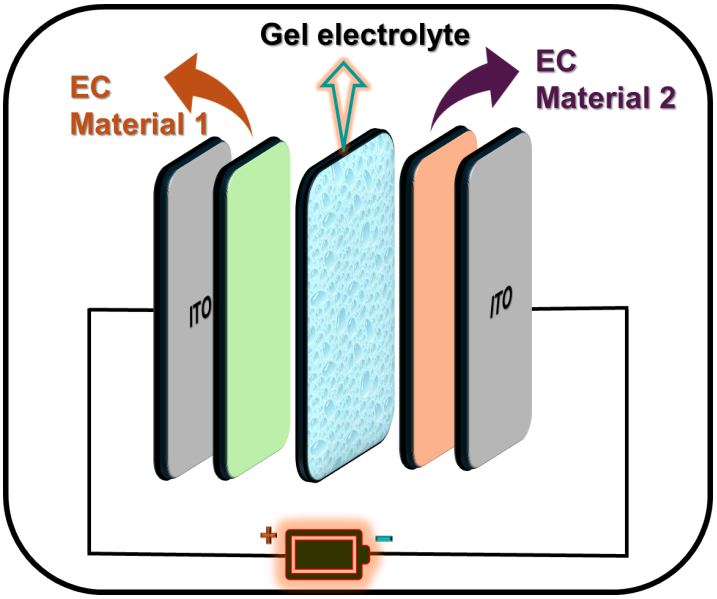

Figure 1.6: Schematic representation five layers of a electrochromic device.

1.3.3 Fabrication of Electrochromic Devices

Since electrochromism is a phenomenon that involves visible light, it is necessary to use transparent materials for the device electrodes to observe this effect. While glass is transparent, it is not conductive. Therefore, glass electrodes are typically coated with a thin layer of Indium-doped Tin Oxide (ITO) or Fluorine-doped Tin Oxide (FTO) to provide conductivity. For flexible electrochromic devices (ECDs), Polyethylene Terephthalate (PET) polymer can be used as an flexible transparent substrate.

An electrochromic device comprises a five-layer structure, as illustrated in Figure 1.6, which includes two electrodes coated with electrochromic material, with an electrolyte layer positioned between the coated electrodes. The electrolyte facilitates the movement of ions for the redox reaction occurring between the electrodes. The electrolyte between the electrodes is maintained in a gel form. To deposit a thin film of electrochromic (EC) material on transparent substrates, various deposition methods can be used, including spin coating, drop casting, electrodeposition, spray pyrolysis, hydrothermal synthesis, and others.

The coated electrodes are assembled using the flip-chip method with double-sided tape. In this process, the tape is cut into a window shape and applied to one of the coated electrodes as illustrated in Figure 1.7. The gel electrolyte is then spread over this electrode, and the second electrode

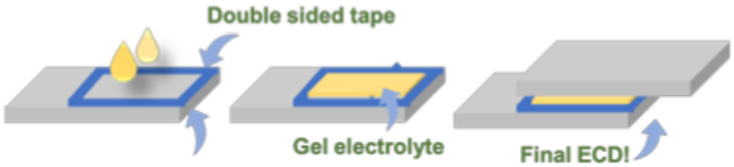

Figure 1.7: Schematic of fabrication of electrochromic device.

is placed on top, ensuring that the conductive sides of both electrodes are facing each other. The assembly is held together with the help of clips, as can be seen in figure 1.8 .

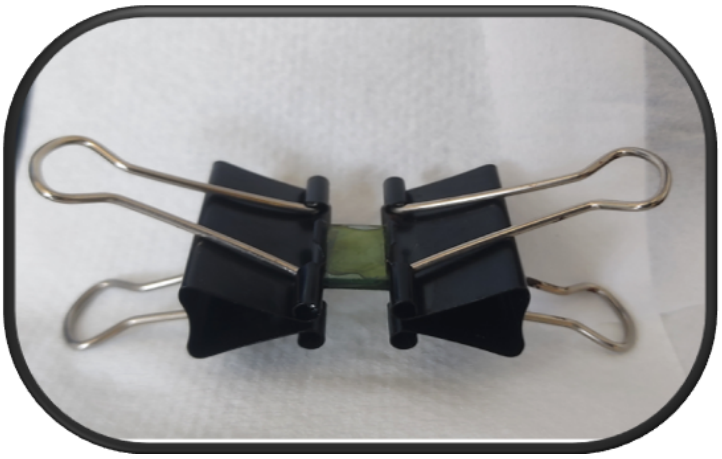

Figure 1.8: Flip Chip Method

We will now examine the various parameters that are used to evaluate the performance of the device.

1.4 Device Performance parameters

To assess the performance of the device, several key parameters need to be considered. These parameters provide insight into the efficiency, functionality, and durability of the electrochromic device.

The following parameters are used to characterize an electrochromic device [19]:

1.4.1 Color contrast (CC)

Color contrast is a measure of the visible optical change, such as absorbance or transmission, expressed in percentage at a specific wavelength

where the maximum color modulation occurs.

$$CC = \frac{T_f - T_i}{T_i} \times 100 \tag{1.1}$$

Where T_f and T_i represent the percentage transmittance values in the device's final and initial optical states, respectively.

Alternatively,

$$CC = \frac{A_i - A_f}{A_i} \times 100 \tag{1.2}$$

Where A_f and A_i represent the percentage absorbance values in the device's final and initial optical states, respectively.

1.4.2 Switching time

The switching time of an electrochromic device refers to the duration required for the device to achieve a 90% transition in absorbance, from one colored state (oxidation state) to another colored state under consideration.

1.4.3 Optical Density (OD)

The optical density (OD) of a material is associated with its optical properties at a specific wavelength and can be expressed in terms of the absorbance (A) and transmittance (T) values of the material at that particular wavelength [19].

$$OD = A = \log_{10}(\frac{1}{T}) \tag{1.3}$$

1.4.4 Coloration efficiency (η_{CE})

Coloration efficiency is defined as the ratio of the change in optical density (OD) of the device during the switching process to the amount of charge injected or extracted per unit area during the switching.

$$\eta_{CE} = \frac{\Delta OD}{Q} \tag{1.4}$$

Here, ΔOD represents the change in optical density between the different optical states, which is calculated as ΔOD= A_i - A_f. In this equation, A_i and A_f correspond to the absorbance values in the initial and final optical states, respectively, while 'Q' refers to the charge density that is inserted or extracted during the switching process.

1.4.5 Cyclic stability

Cyclic stability, or cycle life, measures how long a device can maintain its performance when subjected to continuous coloration and bleaching cycles by applying potential over a specified period of time. It is a crucial parameter for assessing the device's performance qualitatively.

%thispagestyleempty

Chapter 2

Experimental techniques

2.1 Chemicals Used

All chemicals used in this study, including Vanadium oxide (V_2O_5), hydrogen peroxide (H_2O_2), lithium perchlorate ($LiClO_4$), polyethylene oxide (PEO), acetonitrile (ACN, anhydrous, 99%), aniline ($C_6H_5NH_2$), sulfuric acid (H_2SO_4, 98%), MAX Phase (Ti_3AlC_2), hydrofluoric acid (HF), lithium fluoride (LiF), hydrochloric acid (HCl), and analytical-grade reagents such as acetone, 1,2-dichlorobenzene (DCB, anhydrous), ethanol, methanol, and isopropyl alcohol (IPA), were purchased from Alfa Aesar, Sigma Aldrich and were used as received. Indium Tin Oxide (ITO) coated glass electrodes, sourced from Macwin India, were cut into 2×1 cm^2 pieces. The choice of ITO as the substrate was driven by its high conductivity and transparency, which are crucial for electrochromic devices (ECDs).

2.2 Electrode fabrication methods

There are numerous advanced techniques employed to fabricate electrodes, including Chemical Vapor Deposition (CVD), brush coating, inkjet printing (IJP), dip coating, spin coating, hydrothermal synthesis, and electrodeposition, among others.

In this study, electrodes are carefully fabricated using the drop casting and electrodeposition methods, which are discussed in detail in Sections 2.2.1 and 2.2.2. These methods were chosen for their ability to produce high-quality electrodes suited to the study's needs.

2.2.1 Electrodeposition

Electrodeposition is a technique used to deposit a thin material layer onto a conducting substrate's surface by applying an electric field. In principle, the electrolyte solution contains positively charged ions (cations) and negatively charged ions (anions). When an external electric field is applied, the cations move towards the cathode, where they are reduced and deposited as a thin film.This process enables the deposition of a wide range of materials, including metals, metal alloys, semiconductors, metal oxides, nanomaterials, and even conductive polymers onto the substrate [23].

Electrodeposition can be carried out using two methods: **Chronopotentiometry** and **Chronoamperometry**. In chronopotentiometry, a constant current is applied to the electrode, and the change in the electrode potential is studied while the material is being deposited onto the substrate. In chronoamperometry, a constant potential is applied, and the current response of the electrode is measured over time.

The structure and morphology are heavily influenced by the embedded substrate and the electrolyte used for deposition. Electrodeposition offers the opportunity to fine-tune the properties and structure by adjusting various parameters, such as current density, applied potential, and deposition time. As a result, this technique allows for the customisation of a material's surface properties, enabling the exploration of new materials for various applications.

Figure 2.1: Electrodeposition setup in three neck bottle flask.

2.2.2 Drop casting

In drop casting, a droplet of liquid suspension (ink) containing the active chromophore, binder, and solvent is placed onto a substrate, typically a flat surface. The electrode is then fully dried before proceeding with device fabrication (See Figure2.2) [24].

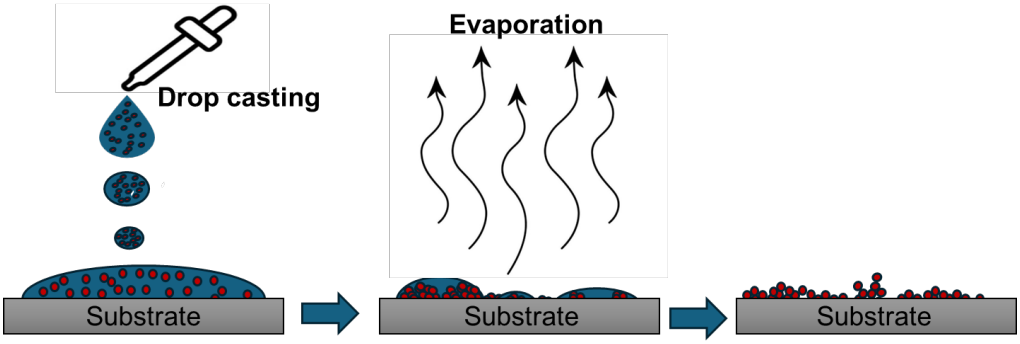

Figure 2.2: Schematic of drop casting method.

It is known for its simplicity, efficiency, and speed, this technique is widely used to prepare electrode surfaces with chemical modifications. This method is suitable for small-scale fabrication but becomes inefficient when applied to large surfaces or in industrial production. [25].

2.3 Prepration of MXene

As previously mentioned, MXene is synthesised through the selective etching of the 'A' layer from the MAX phase material. The MAX phase initially exists as a three-dimensional (3D) structure, which transforms into a two-dimensional (2D) layered material after the removal of the A layer.

In MAX phase materials, the M-X bond is significantly stronger than the M-A bond due to the hybridized (metallic, covalent, and ionic) character of the M-X bond [27]. The etching process begins with the breaking of the M-A bond, followed by the removal of the A layer. Several techniques are available for selectively etching the 'A' layer from the MAX phase material. These techniques include [26]:

1. HF etching
2. Fluoride salt/strong acid etching.

Figure 2.3: Schematic of etching of MAX phase material [26].

3. NH_4HF_2 etching

Since fluorine is hazardous to the environment, there are also fluorine-free etching processes available, which include [26]:

1. Molten salt etching
2. Electrochemical etching
3. Chemical Vapour deposition(CVD) etching

For this study, we synthesised MXene using both the HF and molten salt etching methods, which is discussed in detail, below.

2.3.1 HF etching

HF (Hydrofluoric acid) is widely used to etch the A layer, particularly in aluminum-based MAX phase materials. It was the first etching method employed for the preparation of MXene [28].

0.5 g of MAX phase powder was added to a Teflon beaker containing 10 mL of HF aqueous solution and 10 mL of deionized water. The mixture was stirred for 2 hours at room temperature.

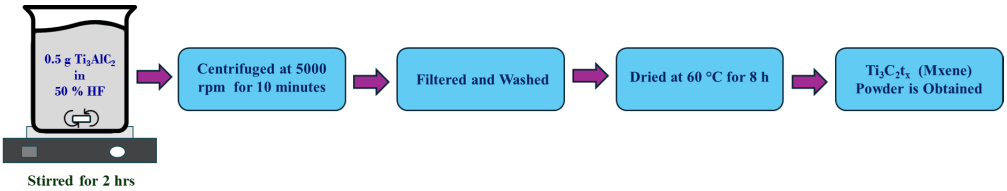

Figure 2.4: Hf etching mthod for MXene synthesis.

The MAX phase undergoes partial decomposition through the following reactions:

$$M_{n+1}AlX_n + 3HF = AlF_3 + M_{n+1}X_n + \frac{3}{2}H_2 \tag{2.1}$$

Afterward, the solids were separated from the supernatant by centrifugation at 5000 rpm for 10 minutes. The filtered material was then washed 2-3 times with deionized water and finally dried at 80°C for 5 hours to obtain MXene powder [28].

2.3.2 LiF + HCl etching

The highly corrosive nature of HF can damage the etched MXene and degrade its surface if the etching conditions are not properly controlled. Furthermore, HF is a hazardous substance, which restricts the broader use of the HF etching method.

Scientists have developed an alternative, safer method for producing HF indirectly, using hydrochloric acid (HCl) and fluoride salts. In this study, we employed Lithium Fluoride salt for the etching process. This method is similar to the previous one, with the primary difference being the presence of metal cations such as Li^+. Because the cations are positively charged and the MXene surface is negatively charged, the cations are inserted between the MXene layers, leading to an increase in the interlayer spacing. The indirect reaction to prepare HF is as follows [28]:

$$LiF + HCl = HF + LiCl \tag{2.2}$$

First, 2.5 mL of deionized water was added to a Teflon container, followed by the addition of 7.5 mL of 12 M HCl and 0.8 g of LiF. Next, 0.5 g of Ti_3AlC_2 was slowly introduced into the solution over 5 minutes while stirring continuously at 300 rpm for 22 hours. Afterward, the suspension was centrifuged at 5000 rpm for 10 minutes. The resulting $Ti_3C_2t_x$ was then filtered and dried at 60°C for 8 hours in an oven under an argon gas flow.

2.4 Characterisation techniques

Characterisation techniques are essential tools used to examine the structure, composition, and properties of materials in great detail. These

methods are crucial in materials science, helping researchers better understand material behaviour and improve the development of new materials. By using these techniques, scientists can identify the best nanomaterials, avoid structural flaws, and enhance material designs for better performance.

Characterisation techniques for nanomaterials can be broadly categorised into two types:

1. Spectroscopic techniques.
2. Microscopic techniques.

2.4.1 Spectroscopic techniques

Spectroscopy refers to a group of techniques that apply various principles to determine the chemical composition, structural variations, and crystal arrangement of materials and their properties. Spectroscopy is founded on the fundamental principle of how light or other forms of electromagnetic radiation interact with matter.

The different types of spectroscopy used to characterise materials include UV-Vis Spectroscopy, Infrared (IR) Spectroscopy, Raman Spectroscopy, X-ray Photoelectron Spectroscopy (XPS), Nuclear Magnetic Resonance (NMR) Spectroscopy, Electron Spin Resonance (ESR) Spectroscopy and X-ray Diffraction (XRD). Out of these, the most common spectroscopic techniques are Raman Spectroscopy and X-ray Diffraction (XRD), which we have discussed briefly in the further sections.

Raman Spectroscopy

Raman spectroscopy is a spectroscopic technique named after physicist, Sir C. V. Raman. It is a powerful technique that looks at how materials vibrate, rotate, and move by scattering light from a laser. It helps us understand the molecular vibrations, which are connected to the chemical makeup and structure of a sample. This method doesn't damage the sample, making it useful for studying both organic and inorganic materials, polymers, and nanomaterials, providing a unique "fingerprint" of the material. It is important for understanding the structure and interactions of molecules without altering the sample.

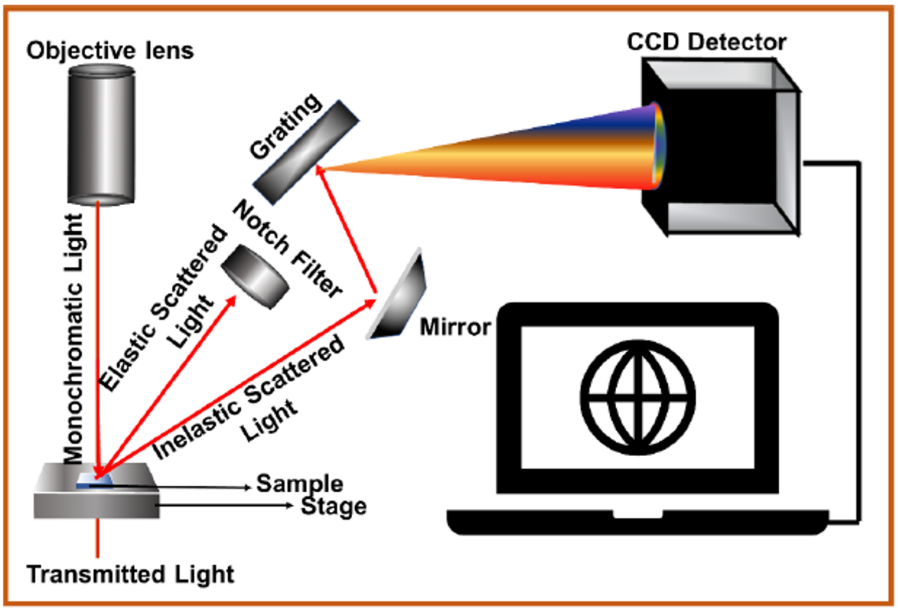

Figure 2.5: Raman spectroscopy setup.

Raman spectroscopy operates by directing a laser beam onto a material. When the laser light interacts with the material's molecules, most of the light is scattered at the same frequency, but a small fraction is scattered at different frequencies. This frequency shift happens because the light interacts with the vibrational modes of the molecules. The change in frequency, known as the "Raman shift", reveals details about the molecular vibrations, enabling the identification of chemical bonds and structures within the material [29].

X-Ray Diffraction

X-ray diffraction (XRD) is a method used to investigate the crystal structure of materials. When X-rays are directed at a sample, they interact with the atoms in the crystal lattice, causing the X-rays to scatter. This scattering produces a diffraction pattern, which, when analysed, reveals details about the atomic arrangement, unit cell size, and overall crystal structure of the material. XRD is commonly used to study both organic and inorganic materials, allowing researchers to identify different phases, determine purity, and measure lattice dimensions.

X-rays are directed at a sample, typically powder or single crystal, which is rotated to interact with different crystallographic planes. The X-rays are diffracted at specific angles based on the crystal structure and detected by

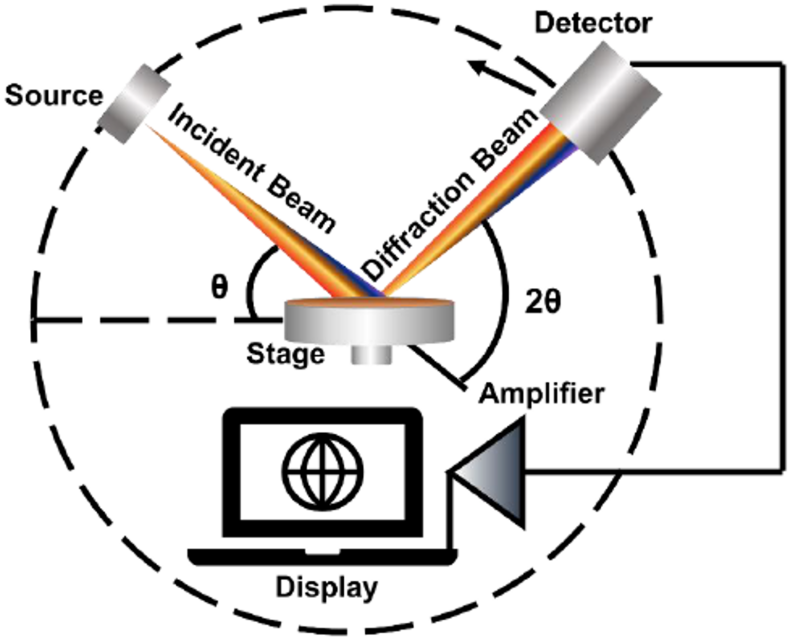

Figure 2.6: X-Ray diffraction setup.

a detector. The resulting diffraction pattern, made up of peaks, reveals information about the material's crystal structure, lattice spacing, and phase composition. By analysing these peaks using Bragg's Law, the atomic arrangement and other properties of the material is determined. A schematic of the XRD setup is shown above in the Figure 2.6.

UV-Visible Absorption Spectroscopy

Absorption spectroscopy is frequently used to determine the absorbance spectrum of specific molecules in solution, as solids, or in thin film form. UV-visible spectroscopy includes both reflectance and absorption spectroscopy. In this study, we focus primarily on absorption spectroscopy [30].

Visible light, which can be detected by the human eye, is electromagnetic radiation with wavelengths ranging from 380 to 780 nanometers. The observed color of a material is complementary to the color of the light it absorbs. When white light strikes a sample, it is partially reflected, giving the sample a white appearance. If the light is fully absorbed, the sample appears black. Selective absorption of a color, like yellow, results in the reflected light lacking yellow, causing the sample to appear blue [30].

The color of a substance is linked to its electronic structure. When it absorbs ultraviolet or visible light, the molecules' electronic state

Wavelength range (nm)[a]	Apparent color	Absorbed color
400–465	Violet	Yellow–green
465–482	Blue	Yellow
482–487	Greenish-blue	Orange
487–493	Blue–green	Red–orange
493–498	Bluish-green	Red
498–530	Green	Red–purple
530–559	Yellowish-green	Reddish-purple
559–571	Yellow–green	Purple
571–576	Greenish-yellow	Violet
576–580	Yellow	Blue
580–587	Yellowish-orange	Blue
587–597	Orange	Greenish-blue
597–617	Reddish-orange	Blue–green
617–780	Red	Blue–green

Table 2.1: The perceived color and the complementary absorbed color.

changes, but only if the transition is possible. In absorption spectroscopy, the "Beer–Lambert law" links the absorption of light to the properties of the material it passes through. Beer's law states that the absorbance of a beam of light in a uniform medium is directly related to the path length (l) and the concentration (c) of the absorbing substance.

Mathematically it can be expressed as :

$$A = \log_{10} \frac{I_0}{I} = \epsilon l c \tag{2.3}$$

Where,

A = Absorbance

I_0 = Incident intensity of light

I = Transmitted intensity of light

ϵ = Molar absorption coefficient

l = Path length

c = Concentration of the sample

A UV-Visible spectrophotometer includes a light source (deuterium for UV and tungsten for visible light), a monochromator to choose specific wavelengths, and a sample holder for the sample. The light passes through the sample, and a detector measures how much light is transmitted. The

data is collected and analysed.

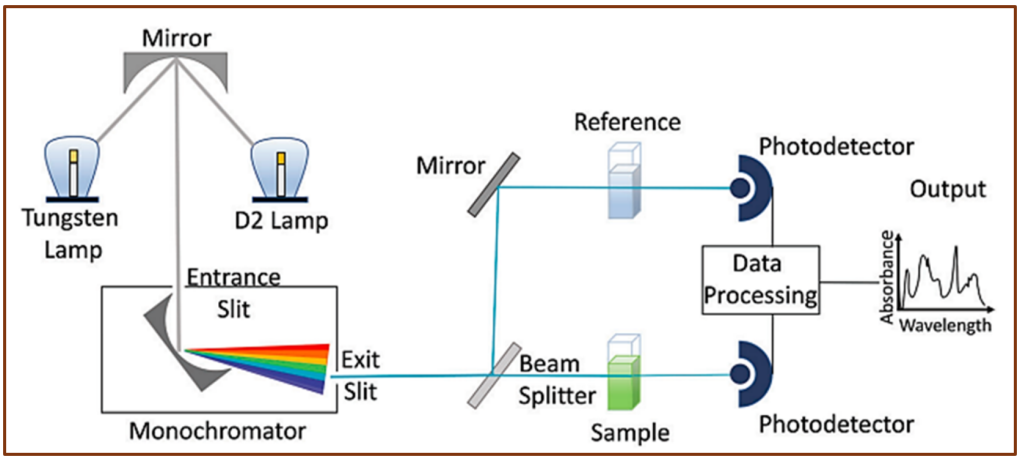

Figure 2.7: UV-Visible spectrophotometer schematic.

2.4.2 Microscopic techniques

Microscopic techniques refer to the methods used to perform microscopy. The basic principle of microscopy is to increase the size and clarity of small objects, making it possible to see details that are invisible to the naked eye.

There are several types of microscopy used to analyse and capture detailed images of specimens. Generally, optical microscopy and electron microscopy are widely available. In this study, we specifically selected scanning electron microscopy (SEM) because optical microscopy is not effective for examining nanomaterials, which are in the nanometer size range. Optical microscopes are limited by the wavelength of visible light, making it difficult to observe structures at such a small scale. On the other hand, scanning electron microscopy uses electron beams with much shorter wavelengths, allowing for much higher resolution and the ability to observe the fine details of nanomaterials. As a result, SEM is better suited for studying materials at the nanoscale.

In our study, we will provide a brief overview of scanning electron microscopy.

Scanning Electron Microscopy (SEM)

Scanning Electron Microscopy is a tool that allows to see the tiny details of the micro and nanoscale world. It can show features and complexities

that light microscopy cannot detect [31].

The SEM setup includes several key components: an electron beam source (electron gun), electromagnetic lenses that function similarly to optical lenses but for focusing the electron beam, scan coils to direct the beam across the sample, and an electron detector to capture backscattered and secondary electrons.

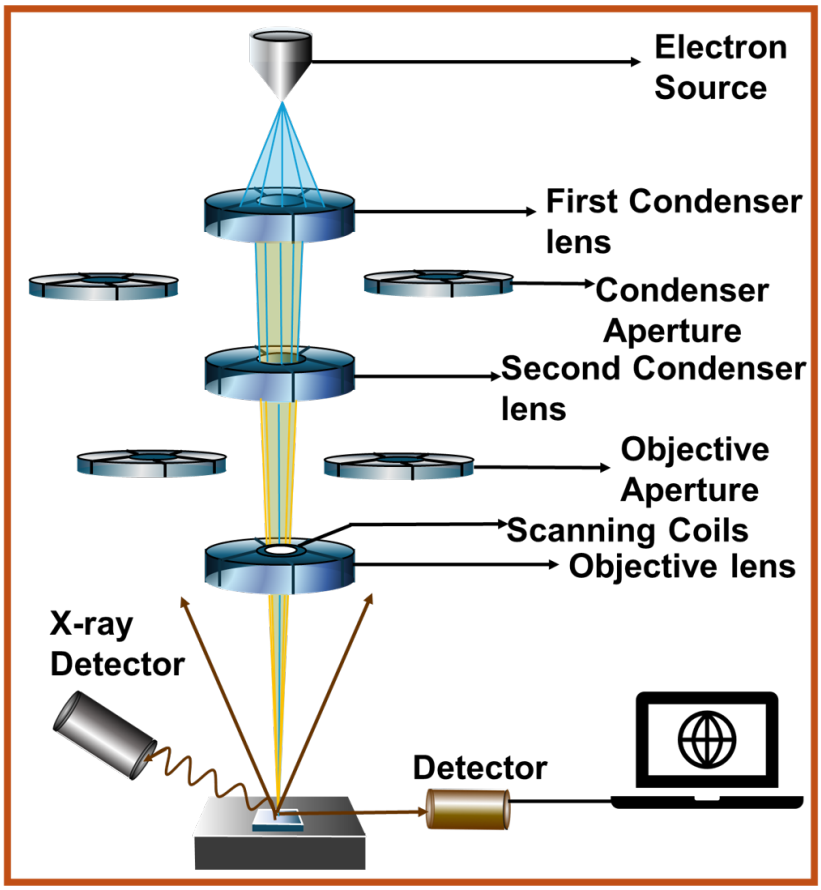

Figure 2.8: Scanning electron microscopy schematic.

The SEM analysis process starts with preparing the sample, which may involve applying a thin conductive coating to reduce charging. A focused electron beam is then directed at the sample and scanned across its surface. The interaction of the beam with the sample produces various signals, such as secondary and backscattered electrons, which are detected to obtain information about the sample's surface and composition. These signals are processed to generate high-resolution images, revealing detailed features at the micro and nanoscale.

2.5 Electrochemistry

Electrochemistry is the study of chemical reactions that involve the movement of electrons. It looks at how chemical changes can produce electrical energy or how electrical energy can cause chemical reactions. This field includes processes like oxidation and reduction, which involve the transfer of electrons, and is important for understanding things like batteries, corrosion, and electroplating [32].

Electrochemical reactions : Electrochemical reactions involves transfer of electrons , leading to changes in the oxidation states of the atoms, ions, or molecules taking part. These reactions are commonly redox reactions, in which one substance undergoes oxidation by losing electrons, while another gains electrons through reduction [20].

Electrochemistry includes a range of techniques such as cyclic voltammetry, electrochemical impedance spectroscopy, chronoamperometry, chronopotentiometry, voltammetry, etc. These methods are applied to explore the dynamics of electrochemical systems, understand reaction mechanisms, evaluate electrode behavior, and study the kinetics of electron transfer. Below, a brief explanation of cyclic voltammetry (CV) is provided.

2.5.1 Cyclic Voltammetry (CV)

Cyclic voltammetry is an electrochemical technique used to examine a molecular species's reduction and oxidation states.

In cyclic voltammetry, the potential of the "Working electrode" is recorded relative to a "Reference electrode", which is kept at a constant potential. The applied potential then generates an excitation signal. The voltage is varied between two fixed potentials (V_1 and V_2) at a constant rate, known as the "Scan Rate". When the potential reaches the maximum boundary value V_2, it is reversed and moves toward the minimum boundary value V_1, completing one cycle of the cyclic voltammetry (CV). The term "Potential Window" refers to the range of applied voltage (V_1 to V_2) over which the potential is varied. The potential window should be selected to ensure that all oxidation and reduction states of the sample are induced. The current response of the analyte is measured at a specific applied potential, and the resulting plot is referred to as a "Voltammogram" [33].

2.6 Poly-Aniline electrode synthesis

Polyaniline (PANI) is a conductive polymer formed by polymerizing aniline, an organic compound. It consists of repeated aniline units and is known for its ability to conduct electricity. Of its three states, emeraldine (EM) is the most stable and the only conductive state, unlike the other two states, leucoemeraldine (LM) and pernigraniline (PG) [34]. The chemical formula for polyaniline is $(C_6H_7N)_x$.

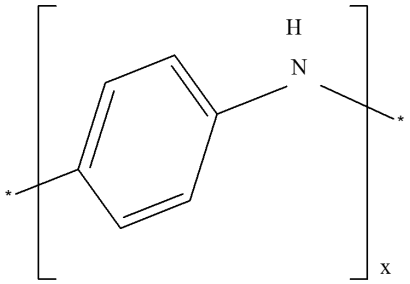

Figure 2.9: Molecular structure of PANI.

The PANI electrode was fabricated through the electrodeposition method, refer to section 2.2.1. A 20 mL mixture of 0.5 M aniline and 1 M sulfuric acid (H_2SO_4) was prepared and diluted with deionized (DI) water. After 10 minutes of continuous stirring, the solution was transferred to a three-necked flask. A 1 cm $\times$ 2 cm ITO electrode were sonicated in an acetone-isopropyl alcohol (IPA) mixture, then dried for use as working electrode in the electrodeposition process. A potential of 0.75 V was applied for 120 seconds to the working electrode to deposit a thin layer of polyaniline (PANI) onto the ITO substrate. All applied potentials were referenced to the Ag/AgCl electrode. The ITO electrode was then rinsed with DI water and dried at 70°C for 30 minutes [35].

2.7 $V_2O_2(OH)_3$ electrode synthesis

$V_2O_2(OH)_3$ is a complex of oxide and hydroxide based on V_2O_5 (Vanadium pentoxide). The complex was formed through the chemical (wet) etching of V_2O_5. The chemical etching procedure is explained below.

Chemical etching

Chemical etching is a wet etching process by which material can be chemically corroded in an isotropic manner, in a certain pattern and at a preferred rate. The goal of the etching process is to dissolve a selective

component of the precursor to obtain the material of our desire.

1.07 g of V_2O_5 was mixed with 40 mL of H_2O_2 and stirred continuously for 10 minutes. The resulting solution was then dried at 100°C in an oven until it transformed into a powder. The obtained powder was then deposited (100 µL) onto the ITO substrate using the drop-casting method, with a dispersion of 2 mg/mL prepared in deionized water. The electrode was then dried at 70°C for 30 minutes [36].

2.8 Device prepration

The electrochromic device consisting of PANI and the V_2O_5 complex was fabricated using the process outlined in Chapter 1 (see Section 1.3.3). The gel form of 1 M $LiClO_4$ electrolyte was prepared using the PEO gel.

Chapter 3

Results and Discussion

3.1 Basic physical characterisation of synthesised materials

After synthesising the materials, i.e., $Ti_3C_2t_x$, $V_2O_2(OH)_3$ and Polyaniline, it is essential to verify that the synthesised material corresponds to the intended composition. To achieve this, we will characterise the materials using the techniques outlined in previous sections, which includes Raman spectroscopy (see Section 2.4.1), X-ray diffraction (see Section 2.4.1), and scanning electron microscopy (see Section 2.4.2). A detailed discussion of the characterisation results for $Ti_3C_2t_x$, $V_2O_2(OH)_3$ and Polyaniline will be presented in subsequent sections.

3.1.1 Characterisation of MXene ($\mathbf{Ti_3C_2t_x}$)

Since MXenes are synthesised through the wet chemical etching of MAX phase materials, a comparative study was conducted to characterise the MXene etched via different chemical etching methods and compartive study with MAX phase and pure MXene. Specifically, the study includes:

- The pristine MAX phase
- A reference sample of pure MXene for comparison
- MXene produced through an alternative fluoride salt etching method (LiF + HCl)
- MXene synthesised through direct etching using hydrofluoric acid (HF)

Raman shift study

To study the vibrational modes and chemical composition of synthesised MXenes ($Ti_3C_2t_x$), MAX phase (Ti_3AlC_2) and pure MXene (Ti_3C_2), Raman spectroscopy has been done using an excitation laser of 532 nm wavelength in backscattering geometry.

Ti_3AlC_2 (MAX phase) shows distinct Raman bands, among which intense bands occurring at 260 cm^{-1} are associated with the vibrations of Ti and Al bonds, and shallow bands occurring at 400 and 600 cm^{-1} are associated with Ti–C bonds. A small peak at 153 cm^{-1} is the E_g vibrational mode of anatase phase TiO_2 particles formed due to spontaneous oxidation of surface titanium atoms [see figure 3.1.(a)] [37].

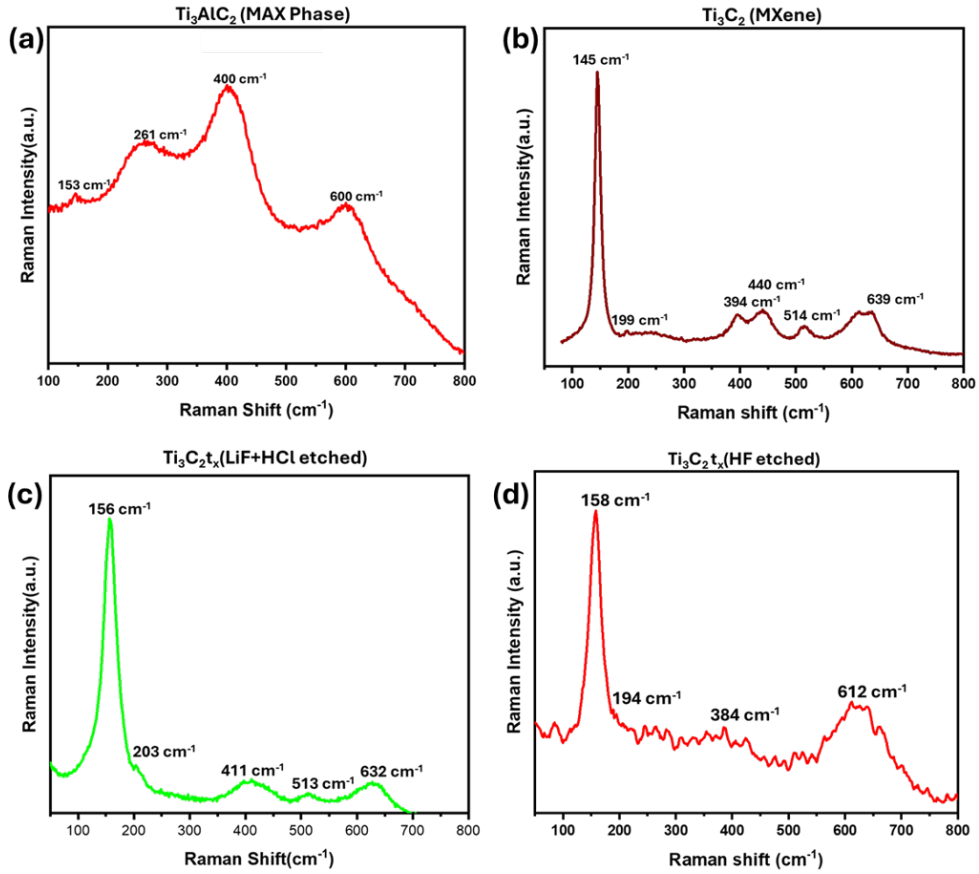

Figure 3.1: Raman spectrum of (a) MAX Phase, (b) Pure MXene, (c) MXene (LiF +HCl etched), (d) MXene (HF etched).

Raman spectra of HF and flouride salt (LiF+HCl) etched MXenes ($Ti_3C_2t_x$) shows the peaks at 145 cm^{-1}, 199 cm^{-1}, 440 cm^{-1} and 639 cm^{-1}. $Ti_3C_2t_x$ [Figure 3.1.(c),(d)] shows a broadened peak around 200 cm^{-1}, which is assigned to the Ti-Al vibrational mode. The peak at 145

cm^{-1} is very intense relative to the band intensity of MAX, which means there is a sufficient amount of TiO_2 [37]. The peaks around 152 cm^{-1} and 632 cm^{-1} correspond to A_{1g} vibration modes for both the carbon layer and titanium outer layer of MXene respectively, in both etched MXenes [38].

MXene etched through hydrofluoric acid (HF) shows the redshift of the peaks when compared with flouride salt (LiF+HCl) etched MXene. Raman spectrum of HF etched MXene is not smooth because of its fluorescent nature. The peak positions in the raman spectra of HF and LiF+HCl etched MXenes confirms the successful synthesis of the compound which matches with the Raman spectrum of pure MXene [Figure 3.1.(b)]

X-Ray diffraction pattern study

Powder X-Ray Diffraction (p-XRD) has been used to validate the crystallinity as well as formation of MXene from MAX phase. XRD pattern of the parent MAX phase and MXenes in the detection range of 15° to 70° is shown in figure 3.2.

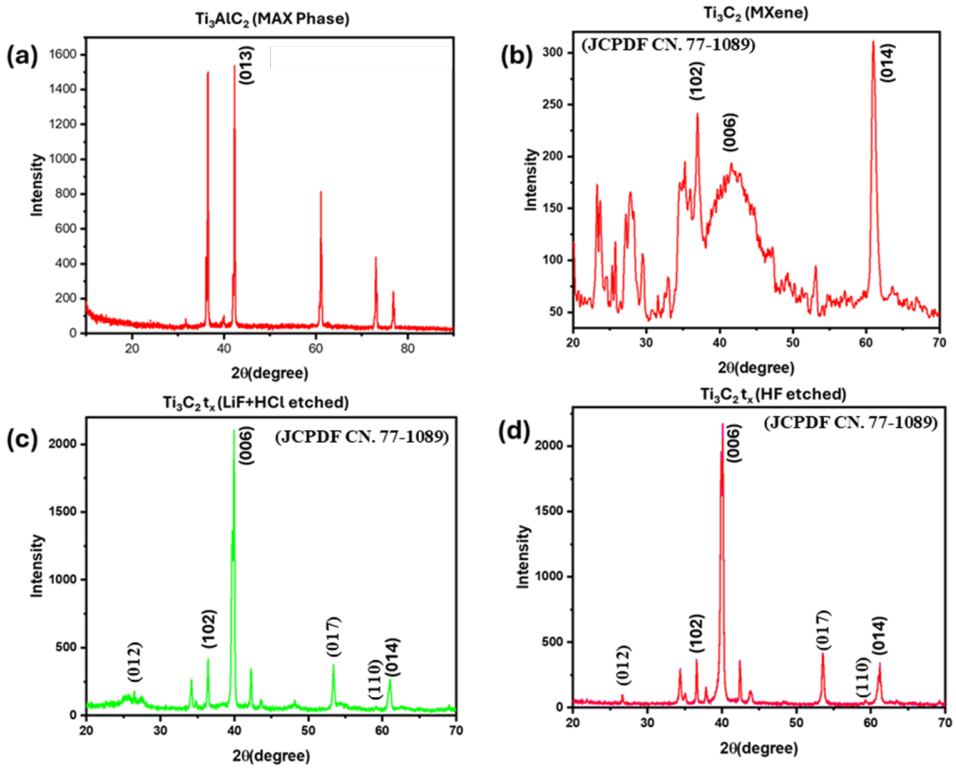

Figure 3.2: Powder X-Ray diffraction pattern of (a) MAX phase, (b) Pure MXene (Ti_3C_2)c (c) MXene (LiF +HCl etched), (d) MXene (HF etched).

In both the etched MXenes, Three characteristic peaks observed around 36°, 40° and 61° correspond to (102), (006), (014) planes, respectively. The increase in the intensity of peaks for $Ti_3C_2t_x$ MXenes showed that crystallinity increases after the removal of aluminum from the MAX phase [39]. XRD peaks around $2\theta = 25°$ indicates the characteristic peak of TiO_2 [38].

The most intense peak around $2\theta = 41.8°$ in $Ti_3C_2t_x$ MXenes (Figure 4c, d) corresponds to the (014) plane of the hexagonal structure. Hence, The experimental XRD patterns confirm the hexagonal structure of etched MXenes [39].

FESEM micrographs

The MXene ($Ti_3C_2t_x$) etched using HF [Figure 3.3.(b)] and MAX phase [Figure 3.3.(a)] has been characterised using FESEM, the formation of nanosheet having a few nanometers thick sheets, providing more active sites for the transport of electrolyte ions which is helpful for energy storage application.

The FESEM image of the MXene sample shows limited visibility of individual sheets, suggesting incomplete exfoliation. This may require additional exfoliation or sonication to better separate the MXene layers and improve sheet dispersion.

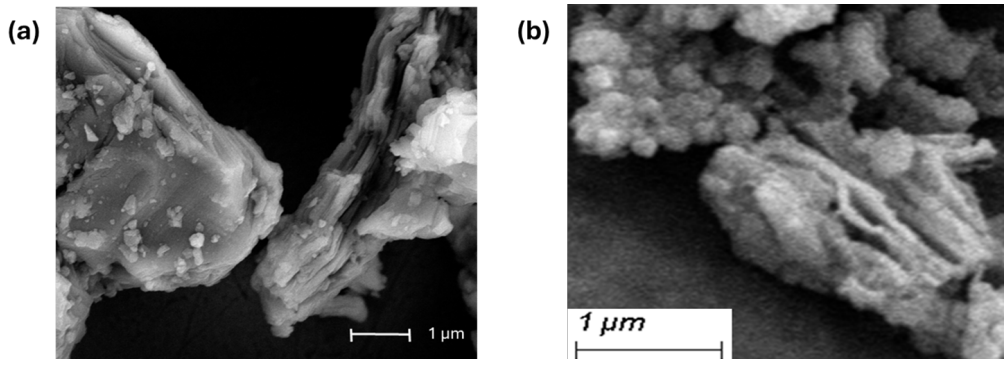

Figure 3.3: FESEM micrographs of (a) MAX phase, (b) HF etched MXene.

The above findings confirms the successful etching of the MAX phase, resulting in pure $Ti_3C_2t_x$ MXene using both the synthesis mechanisms.

3.1.2 Characterisation of $V_2O_2(OH)_3$

The powder $V_2O_2(OH)_3$ was utilized for purity confirmation through Raman spectroscopy. The Raman spectrum of the V_2O_5 complex [Figure

3.4.(a)] displays nine characteristic peaks at 153, 215, 262, 324, 343, 415, 513, 707, and 885 cm^{-1}. The peaks observed in the 650 to 400 cm^{-1} range are attributed to symmetric and antisymmetric stretching vibrations of V–O–V bridging bonds. The peak near 1000 cm^{-1} is associated with the characteristic feature of orthorhombic V_2O_5. The XRD pattern of $V_2O_2(OH)_3$ reveals an amorphous phase as evidenced by the broad peaks in the XRD [Figure 3.4.(b)] [36].

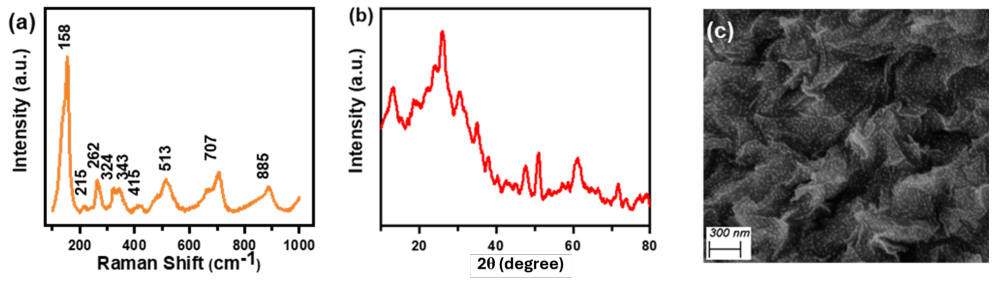

Figure 3.4: Characterization of $V_2O_2(OH)_3$: (a) Raman spectroscopy (b) X-Ray Diffraction, and (c) Scanning Electron Microscopy.

The surface morphology of the complex was examined using SEM micrographs [see Figure 3.4.(c)]. The micrographs show a uniform distribution of micro-sized nanoflake-like structures, which enhance the electrochemical properties of the $V_2O_2(OH)_3$ complex.

3.1.3 Characterisation of Polyaniline

The Raman spectrum was used to examine the electrodeposited polyaniline electrode [Figure 3.5.(a)].The characteristic peak of PANI appears at 1187 cm^{-1}, corresponding to the C-H bending mode. The peak at 1355 cm^{-1} represents C-N^+ vibrations, while the peaks at 1512 and 1591 cm^{-1} are attributed to C=N and C-C stretching vibrations, respectively [40].

The SEM micrographs of the electrode [Figure 3.5.(b)] shows the agglomeration of PANI molecules, and due to the shorter electrodeposition time, the film is unevenly deposited on the ITO electrode.

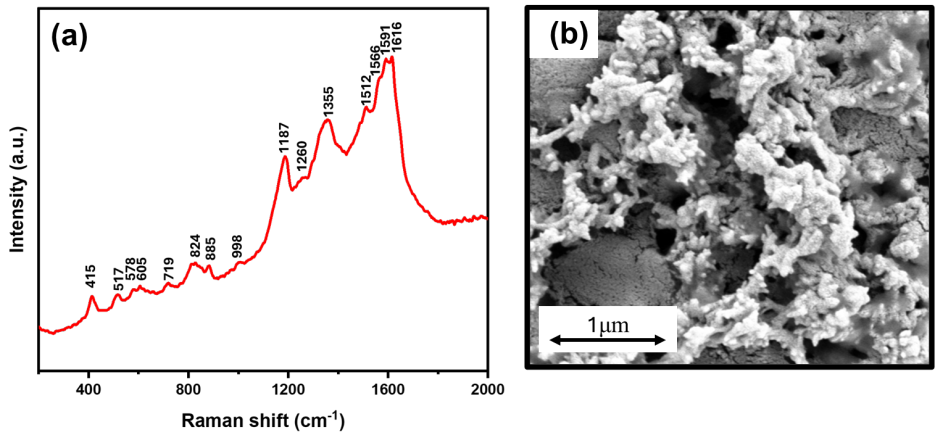

Figure 3.5: Characterization of PANI : (a) Raman spectroscopy (b) Scanning Electron Microscopy.

3.2 Cyclic Voltammetry

The electrochemical analysis of the electrode will help explore the potential applications of these materials. This section will focus on discussing the CV voltammograms of MXene along with the two electrodes [$V_2O_2(OH)_3$ and PANI].

3.2.1 $Ti_3C_2t_x$

CV was conducted to investigate the electrochemical behaviour of the synthesised $Ti_3C_2t_x$ MXene, using 1 M KOH as the electrolyte. The measurements were performed within a potential window ranging from -1.5 V to +1.5 V (v/s. Ag/AgCl).

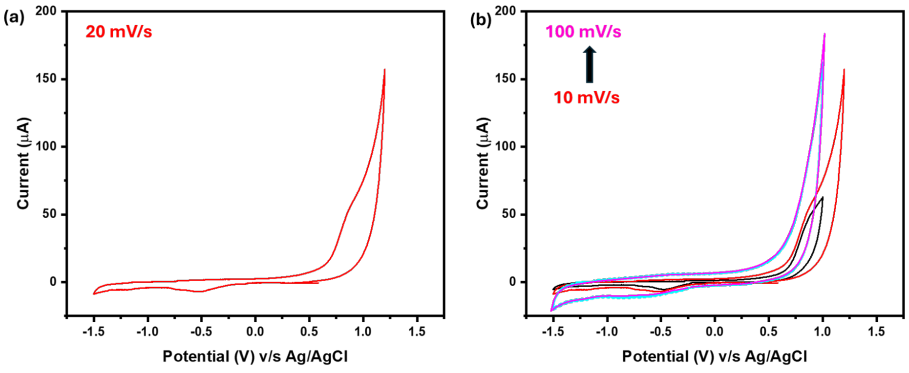

Figure 3.6: CV Curve of $Ti_3C_2t_x$ (a) at scan rate 20mV/s, and (b) Varying scan rates (10 to 100 mV/s).

The CV curve [figure 3.6.(a)] exhibited a distinct anodic peak at approximately +0.8 V and a cathodic peak near –0.5 V. These redox features are indicative of pseudocapacitive behaviour, confirming the presence of faradaic charge storage mechanisms in the MXene material.

3.2.2 $V_2O_2(OH)_3$

Figure 3.7 shows the CV voltammograms of $V_2O_2(OH)_3$ at various scan rates (10, 20, 30, 40, and 50 mV/s) in 1M $LiClO_4$ electrolyte within the potential range of -1.5 V to 2.0 V (versus Ag/AgCl electrode). A dark blue color is observed when $V_2O_2(OH)_3$ is fully reduced, while a reddish dark color appears when it is fully oxidized.

Increase in the current density proportionally increases the charge flow in the electrochemical process, resulting into a larger area under the CV curve. Furthermore, the increased current density reduces the time available for ions to intercalate within the electrode, causing the complete intercalation of ions to occur at a shifted potential.

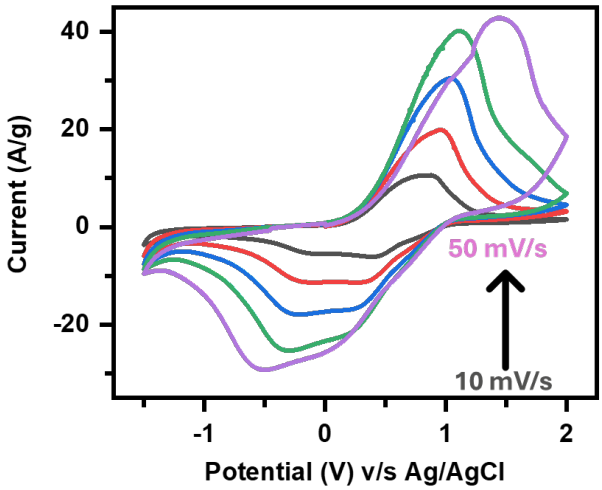

Figure 3.7: CV Curve of $V_2O_2(OH)_3$ at varying scan rates (10 to 50 mV/s).

3.2.3 Polyaniline

The redox behavior of PANI electrode is studied through the scan rate-dependent CV voltammograms (10 to 100 mV/s) in 1M $LiClO_4$ electrolyte, within the potential window of -0.5 V to 1.5 V, are shown in the figure 3.8.

Polyaniline displays three stable colored forms, with the redox peak at +0.7 V representing the oxidation from the emeraldine (green) state to the pernigraniline (blue) state of PANI which reduces again to green state at 0.6 V. The peak around -0.1 V results the Yellow color of PANI electrode [34].

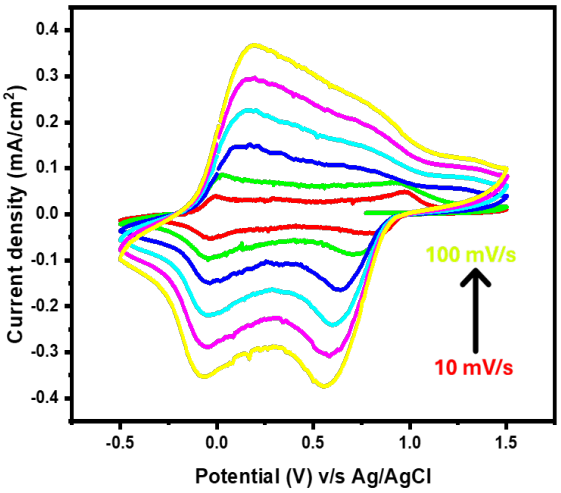

Figure 3.8: CV Curve of Polyaniline at varying scan rates (10 to 100 mV/s).

3.3 Device fabrication

After studying the CV voltammograms of the materials, we found that both electrodes show the ability to change color when exposed to both positive and negative potentials, meaning they are ambipolar in nature. This property makes them suitable for use in electrochromic devices (ECDs). If we use one electrode as a p-type electrochromic material and the other as an n-type material, the device can display a noticeable color contrast. The combination of both types of materials in the ECD can enhance the visual effect and performance of the device.

To test the compatibility of these two electrodes, an electrochromic device (ECD) was prepared with a $V_2O_2(OH)_3$ electrode under positive bias and a PANI electrode under negative bias. The electrolyte used was a 1M $LiClO_4$ solution mixed with PEO gel, which helps maintain the electrolyte in a gel consistency. This prevents the electrolyte from leaking out of the device, a limitation that would occur with a liquid electrolyte.

In the "OFF" state, i.e., $V_2O_2(OH)_3$ electrode at +1.5V and PANI

electrode at -1.5 V, the $V_2O_2(OH)_3$ electrode turns red, whereas the PANI electrode becomes light yellow. In this state, the combination of red and light yellow results in a lighter orange color [Figure 3.9(a)]. In the "ON" state, i.e., $V_2O_2(OH)_3$ electrode at -1.5V and PANI electrode at +1.5 V of the device, the PANI electrode turns dark blue, while the $V_2O_2(OH)_3$ electrode becomes blue. When both electrodes are activated, the device appears dark blue. This combination of colors in this state can be seen in the Figure 3.9(b).

The device also retains its reversibility, meaning it can be switched back to the "OFF" state by reversing the applied potentials. This allows the device to cycle between the "ON" and "OFF" states.

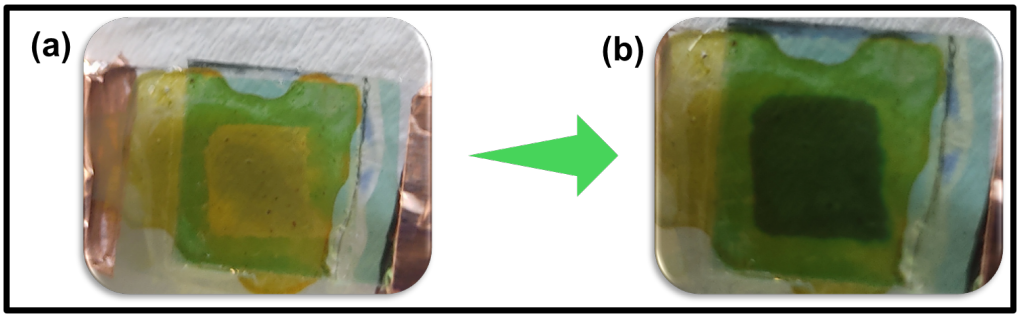

Figure 3.9: The Bi-Layer ECD in : (a) "OFF" state and (b) "ON" state

3.4 Device Performance

Since the device shows a good color contrast qualitatively, we now need to quantify its performance using the parameters outlined in Chapter 1 (section 1.4). This will provide a more detailed and objective assessment of the device's effectiveness and efficiency.

3.4.1 UV-Visible Spectroscopy

The UV-Visible spectrum was measured using a UV-Vis spectrophotometer in the "ON", "OFF", and unbiased states of the electrochromic device. Transmittance was recorded at different wavelengths to study the device's behavior in these states.

The device shows a 75% color contrast (CC) @ wavelength 636nm between the ON and OFF states, which is a positive indication of its good

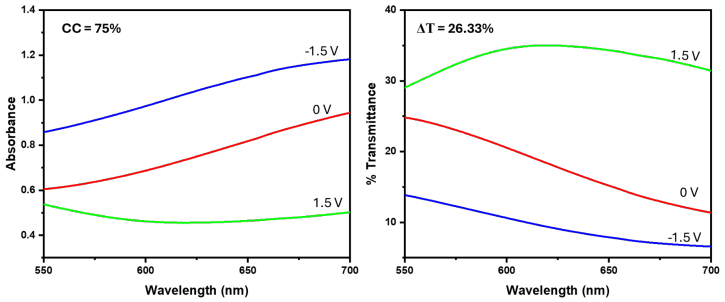

Figure 3.10: UV-Visible spectrum of the electrochromic device (ECD) showing (a) Absorbance and (b) Transmittance as functions of wavelength.

performance for an electrochromic device (ECD), along with a transmittance difference (ΔT) value of 26.33%.

3.4.2 Switching Time

At a wavelength of 636 nm, an electrochromic switching cycle of 20 seconds was recorded, consisting of 10 seconds for coloration and 10 seconds for bleaching [figure 3.11.(a)].

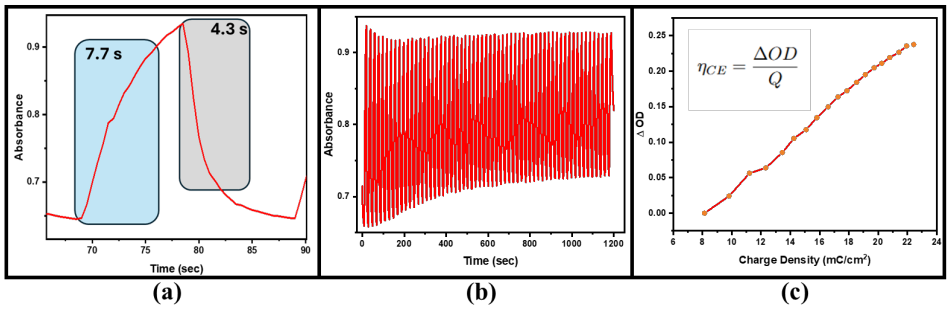

Figure 3.11: Device performance parameters: (a) Switching time, (b) Stability, (c) Coloration efficiency.

The device exhibited a switching time of 7.7 seconds and a bleaching time of 4.3 seconds. It was observed that even after the full 10 seconds of coloration, the absorbance did not reach saturation. This indicates the charge storage behaviour of the $V_2O_2(OH)_3$ material, suggesting that the device requires a longer duration to attain a fully charged state—i.e., to reach its maximum or saturation absorbance.

3.4.3 Stability

The device was subjected to 60 switching cycles over a duration of 1200 seconds, during which the absorbance profile was recorded [figure 3.11.(b)]. After a few initial cycles, a gradual increase was observed in the minimum absorbance level, i.e., the absorbance in the device's OFF state.

This behaviour may be attributed to progressive charge accumulation within the device. It is likely that the 10-second bleaching interval is insufficient for complete discharge, resulting in residual charge being carried over into subsequent cycles. Consequently, the device begins each new cycle in a partially charged state, leading to a higher baseline absorbance compared to the initial cycles. This phenomenon suggests an increase in stored charge during the OFF state over time.

3.4.4 Coloration efficiency (η_{CE})

The slope of the graph plotting the change in optical density against the corresponding charge supplied represents the colouration efficiency of the device, which was calculated to be 18 cm^2 C^{-1} in this study [figure 3.11.(c)].

However, due to the observed charge storage behaviour of the device, the total charge required over time to achieve a given optical modulation increases. As colouration efficiency is inversely proportional to the charge consumed to attain a specific coloured state, this increase in charge input results in a decrease in the effective colouration efficiency of the device.

3.4.5 Summary and shortcomings

Based on the data recorded at a wavelength of 636 nm and within the potential window of +1.5 V to –1.5 V, the overall performance of the device was assessed as moderate. The key observations are as follows:

- a high optical contrast of approximately 75%,
- a colouration time of 7.7 seconds and a bleaching time of 4.3 seconds,
- a moderately stable switching pattern over repeated cycles, and
- a colouration efficiency of 18 cm^2 C^{-1}.

Despite these favourable attributes, the switching speed remains relatively slow, which is a critical parameter for high-performance electrochromic devices. Moreover, the stability pattern displays noticeable deviation from the initial cycles, indicating suboptimal cycling durability. These limitations highlight the need for further investigation and optimisation. Accordingly, subsequent efforts in this study will focus on addressing these shortcomings to improve the device's electrochromic performance.

3.5 Doping of MXene for Enhanced Device Performance

To address the limitations in switching time and stability observed in the electrochromic device, $Ti_3C_2t_x$ MXene was explored as a dopant. MXene offers several characteristics that may contribute to enhanced electrochemical performance.

The rationale for its incorporation is based on the following considerations:

- **Two-dimensional layered structure** – MXene's 2D nature allows for increased ion accessibility and potential intercalation between layers, which may support improved electrochemical response.
- **Porous morphology** – The inherent porosity of MXene can facilitate ion transport and promote more efficient intercalation and deintercalation processes during switching cycles.

These properties suggest that doping with MXene could provide incremental improvements in the switching behaviour and cycling stability of the device.

Optimising Doping wt%

Since MXene appears black in colour, it does not exhibit intrinsic colour-changing properties. As a result, doping with MXene poses a potential risk of reducing the device's colour contrast. To mitigate this, it is necessary to optimise the amount of MXene incorporated so as to improve key electrochromic parameters, such as switching time and cycling stability without causing significant compromise to the overall colour contrast of the device.

Doping (wt%)	Electrochromic performance
1	~10%
0.5	~ 20%
0.1	52%

Table 3.1: Optimising doping wt% of MXene ($Ti_3C_2t_x$).

The dopant weight percentage was optimised and shows a decent colour contrast with 0.1 wt% doping (Table 3.1).

3.5.1 Effect on Color Contrast (CC%)

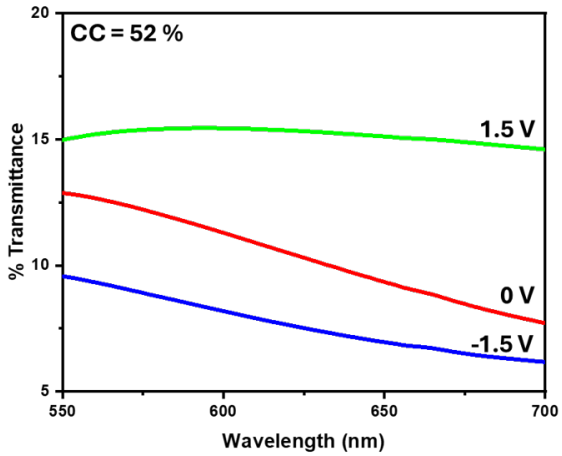

Figure 3.12: Colour contrast of device after doping 0.1wt% MXene.

The colour contrast of the device decreased to 52% (figure 3.12), which can be attributed to the non-electrochromic nature and inherently black appearance of the dopant material.

3.5.2 Effect on Switching time

As observed from the data obtained for the MXene-doped device under the same experimental conditions as the undoped device, and recorded using a UV-Vis spectrophotometer [figure 3.13.(a)], the switching times were improved, with a coloration time reduced to 5.5 seconds and a bleaching time reduced to 2.6 seconds.

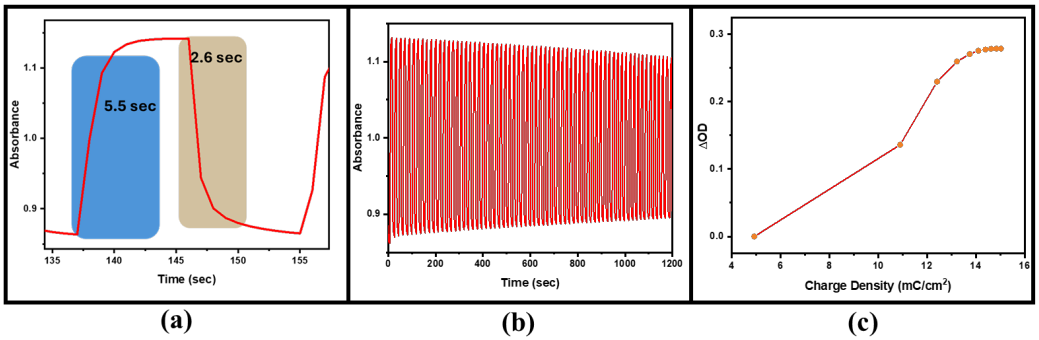

Figure 3.13: Device performance parameters after doping $Ti_3C_2t_x$: (a) Switching time, (b) Stability, (c) Coloration efficiency.

Hence, the hypothesis that MXene incorporation would result in faster switching times, attributed to its porous structure has been validated by the experimental data.

3.5.3 Effect on Stability

As shown in figure 3.13.(b), the device exhibits an improved stability pattern following doping. This enhancement can be attributed to the dopant providing a more efficient pathway for the intercalation and deintercalation of electrolyte ions.

The issue of progressive charge accumulation, previously observed as a result of insufficient bleaching time and reflected as an increasing baseline absorbance in successive cycles appears to be resolved following MXene doping. The improved performance can be attributed to the MXene providing more efficient pathways for the intercalation and deintercalation of charges, thereby enabling more complete discharge within the given switching interval.

3.5.4 Effect on Coloration efficiency (η_{CE})

As determined from the slope of the graph shown in figure 3.13.(c), the coloration efficiency of the doped device was calculated to be 40 cm^2 C^{-1}.

This increase in coloration efficiency can be attributed to a greater change in optical density. Following doping, the ions are intercalated more rapidly, allowing the device to reach its saturation state more effectively. As a result, the maximum optical density is achieved within the switching interval, which was not observed in the undoped device.

3.5.5 Summary

Following the doping of 0.1 wt% MXene into the device, an overall enhancement in electrochromic performance was observed, with the exception of a slight reduction in color contrast. The improved parameters are summarised as follows:

- The switching time was reduced to 5.5 seconds for colouration and 2.6 seconds for bleaching.
- Saturation in absorbance was observed within the switching cycle, indicating more complete charge transfer.
- The device exhibited improved stability over repeated cycles.

Chapter 4

Conclusion and Future Objectives

4.1 Conclusion

Over the course of this year-long study, we investigated the properties of two-dimensional (2D) materials, with a particular focus on the recently discovered material known as MXene, as well as its precursor, the MAX phase material. The study involved the synthesis of MXene from its MAX phase parent compound and included a survey of its potential applications across various fields.

We successfully synthesised MXene ($Ti_3C_2t_x$) using two distinct approaches. The first involved direct chemical etching of the MAX phase with hydrofluoric acid, while the second employed an alternative route wherein hydrofluoric acid was generated in situ by reacting lithium fluoride (LiF) with hydrochloric acid (HCl). The synthesised $Ti_3C_2t_x$ MXenes were characterised and compared against a reference sample of conventionally synthesised MXene to assess structural and compositional consistency. Additionally, cyclic voltammetry (CV) was performed at various scan rates to investigate and verify the electrochemical behaviour of the synthsised materials. In the latter part of the study, we explored the potential application of MXene in the field of electrochromism an area in which its use has not yet been extensively investigated.

To investigate the effect of MXene on electrochromic behaviour, it was essential to select an electrochromic material that has not been extensively studied, in order to preserve the novelty of the work. During

the literature survey, a recently identified vanadium-based complex, $V_2O_2(OH)_3$, was found to exhibit promising charge storage properties and decent electrochromic properties. Consequently, this material was chosen as the focus for our electrochromic study. Given that $V_2O_2(OH)_3$ is an ambipolar electrochromic material, polyaniline (PANI), which is a well-known conducting polymer, was also examined to assess its feasibility within the electrochromic device setup.

The $V_2O_2(OH)_3$ material was synthesised via a simple drop-casting method, while polyaniline (PANI) was deposited using an electrodeposition technique, both using indium tin oxide (ITO) as the substrate. The synthesised materials were then physically characterised using X-ray diffraction (XRD), scanning electron microscopy (SEM), and Raman spectroscopy. Following compositional and structural verification, the materials were utilised as electrodes in the fabrication of the electrochromic device.

The electrochromic device was then evaluated based on various electrochromic parameters using a UV-Vis spectrophotometer. The study demonstrated a high color contrast of 75% at a wavelength of 636 nm within the potential window of +1.5 V to –1.5 V. However, the switching time of 7.7 seconds and bleaching time of 4.3 seconds were relatively slow and are attributed to the charge storage characteristics of the $V_2O_2(OH)_3$ material. In addition, the device exhibited a moderate stability pattern over repeated cycles and a colouration efficiency of 18 cm^2 C^{-1}.

The relatively large switching time posed a significant challenge for the electrochromic device, as it is a key parameter for performance. To address this, MXene was employed as a dopant in the electrochromic material, utilising on its porous nature, which facilitates faster intercalation and deintercalation of ions, thereby improving the switching dynamics and hence the stability of the device.

After doping 0.1 wt% MXene ($Ti_3C_2t_x$) with $V_2O_2(OH)_3$, the subsequently fabricated device exhibited a reduced colour contrast of 52%, which can be ascribed to the non-electrochromic nature and inherently black appearance of MXene. However, as anticipated, the switching performance improved, with the coloration time reduced to 5.5 seconds and the bleaching time to 2.6 seconds. The stability of the device was also enhanced,

likely due to more complete discharge of stored charge during each cycle. Additionally, the coloration efficiency increased to 40 cm^2 C^{-1}, indicating improved optical modulation per unit charge.

4.2 Future Scope

MXene, as a recently discovered class of two-dimensional (2D) materials, holds significant potential, with hundreds of new variants yet to be synthesised and characterised. Future research may focus on exploring various types of MXenes and their interaction with different electrochromic materials to better understand their compatibility and influence on device performance.

Additionally, the effect of MXenes on infrared (IR) shielding electrochromic devices could be investigated, with the aim of enhancing their functional parameters. Given MXene's pseudocapacitive behaviour, it also presents a promising opportunity for study within the fields of batteries and supercapacitors.

Furthermore, by combining the principles of electrochromism and charge storage, MXenes could facilitate the development of multifunctional electrochromic supercapacitors, paving the way for integrated energy storage and smart display applications.

Bibliography

[1] Ankur Gupta, Tamilselvan Sakthivel, and Sudipta Seal. Recent development in 2d materials beyond graphene. *Progress in Materials Science*, 73:44–126, 2015.

[2] Lokanath Patra and Ravindra Pandey. Mechanical properties of 2d materials: A review on molecular dynamics based nanoindentation simulations. *Materials Today Communications*, 31:103623, 2022.

[3] Qijie Ma, Guanghui Ren, Kai Xu, and Jian Zhen Ou. Tunable optical properties of 2d materials and their applications. *Advanced Optical Materials*, 9(2):2001313, 2021.

[4] Deji Akinwande, Nicholas Petrone, and James Hone. Two-dimensional flexible nanoelectronics. *Nature communications*, 5(1):5678, 2014.

[5] Jérémy Come, Michael Naguib, Patrick Rozier, Michel W Barsoum, Yury Gogotsi, P-L Taberna, Mathieu Morcrette, and Patrice Simon. A non-aqueous asymmetric cell with a ti2c-based two-dimensional negative electrode. *Journal of the Electrochemical Society*, 159(8):A1368, 2012.

[6] Can Zhou, Xiaohan Zhao, Yingshuo Xiong, Yuanhan Tang, Xintao Ma, Qian Tao, Changmei Sun, and Wenlong Xu. A review of etching methods of mxene and applications of mxene conductive hydrogels. *European Polymer Journal*, 167:111063, 2022.

[7] Michael Naguib, Joseph Halim, Jun Lu, Kevin M Cook, Lars Hultman, Yury Gogotsi, and Michel W Barsoum. New two-dimensional niobium and vanadium carbides as promising materials for li-ion batteries. *Journal of the American Chemical Society*, 135(43):15966–15969, 2013.

[8] Jizhen Zhang, Na Kong, Simge Uzun, Ariana Levitt, Shayan Seyedin, Peter A Lynch, Si Qin, Meikang Han, Wenrong Yang, Jingquan Liu,

et al. Scalable manufacturing of free-standing, strong ti3c2tx mxene films with outstanding conductivity. In *MXenes*, pages 519–538. Jenny Stanford Publishing, 2023.

[9] Hao Xu, Aobo Ren, Jiang Wu, and Zhiming Wang. Recent advances in 2d mxenes for photodetection. *Advanced Functional Materials*, 30(24):2000907, 2020.

[10] Yanbao Guo, Xuanli Zhou, Deguo Wang, Xiaqing Xu, and Quan Xu. Nanomechanical properties of ti3c2 mxene. *Langmuir*, 35(45):14481–14485, 2019.

[11] Jin-Cheng Lei, Xu Zhang, and Zhen Zhou. Recent advances in mxene: Preparation, properties, and applications. *Frontiers of Physics*, 10:276–286, 2015.

[12] Changlei Xia, Haoran Ye, Aejung Kim, Abbas Sabahi Namini, Suiyi Li, Seyed Ali Delbari, Joo Young Park, Dokyoon Kim, Quyet Van Le, Rajender S Varma, et al. Recent catalytic applications of mxene-based layered nanomaterials. *Chemosphere*, 325:138323, 2023.

[13] Lujie Yin, Yingtao Li, Xincheng Yao, Yanzhou Wang, Lin Jia, Qiming Liu, Junshuai Li, Yali Li, and Deyan He. Mxenes for solar cells. *Nano-Micro Letters*, 13:1–17, 2021.

[14] Armin VahidMohammadi, Johanna Rosen, and Yury Gogotsi. The world of two-dimensional carbides and nitrides (mxenes). *Science*, 372(6547):eabf1581, 2021.

[15] MW Barsoum. A new class of solids: Thermodynamically stable nanolaminates. *Prog. Solid State Chem*, 28:201, 2000.

[16] Xin Lei and Naiming Lin. Structure and synthesis of max phase materials: a brief review. *Critical Reviews in Solid State and Materials Sciences*, 47(5):736–771, 2022.

[17] Jesus Gonzalez-Julian. Processing of max phases: From synthesis to applications. *Journal of the American Ceramic Society*, 104(2):659–690, 2021.

[18] John R Platt. Electrochromism, a possible change of color producible in dyes by an electric field. *The Journal of Chemical Physics*, 34(3):862–863, 1961.

[19] Rajesh Kumar, Devesh K Pathak, and Anjali Chaudhary. Current status of some electrochromic materials and devices: a brief review. *Journal of Physics D: Applied Physics*, 54(50):503002, 2021.

[20] Monika Wałęsa-Chorab, Radosław Banasz, Damian Marcinkowski, Maciej Kubicki, and Violetta Patroniak. Electrochromism and electrochemical properties of complexes of transition metal ions with benzimidazole-based ligand. *RSC advances*, 7(80):50858–50867, 2017.

[21] Bhumika Sahu, Love Bansal, Nikita Ahlawat, Anjali Ghanghass, Deb Kumar Rath, Subin Kaladi Chondath, Suchita Kandpal, Ravi Bhatia, Ivaturi Sameera, and Rajesh Kumar. Mixed chalcogenides nanoflakes' infrared cutting effect: Utilization in thermal soothing electrochromic goggles. *ACS Applied Optical Materials*, 2(10):2128–2136, 2024.

[22] Tanushree Ghosh, Suchita Kandpal, Chanchal Rani, Anjali Chaudhary, and Rajesh Kumar. Recipe for fabricating optimized solid-state electrochromic devices and its know-how: challenges and future. *Advanced Optical Materials*, 11(12):2203126, 2023.

[23] P Sebastin, V Climent, JM Feliu, and E Gomez. Ionic liquids in the field of metal electrodeposition. 2018.

[24] Archana Kaliyaraj Selva Kumar, Yifei Zhang, Danlei Li, and Richard G Compton. A mini-review: How reliable is the drop-casting technique? *Electrochemistry Communications*, 121:106867, 2020.

[25] Veena Singh, Sudhanshu Kuthe, and Natalia V Skorodumova. Electrode fabrication techniques for li ion based energy storage system: a review. *Batteries*, 9(3):184, 2023.

[26] Can Zhou, Xiaohan Zhao, Yingshuo Xiong, Yuanhan Tang, Xintao Ma, Qian Tao, Changmei Sun, and Wenlong Xu. A review of etching methods of mxene and applications of mxene conductive hydrogels. *European Polymer Journal*, 167:111063, 2022.

[27] Zhimei Sun, Denis Music, Rajeev Ahuja, Sa Li, and Jochen M Schneider. Bonding and classification of nanolayered ternary carbides. *Physical Review B—Condensed Matter and Materials Physics*, 70(9):092102, 2004.

[28] Michael Naguib, Olha Mashtalir, Joshua Carle, Volker Presser, Jun Lu, Lars Hultman, Yury Gogotsi, and Michel W Barsoum. Two-dimensional transition metal carbides. *ACS nano*, 6(2):1322–1331, 2012.

[29] Andrea Orlando, Filippo Franceschini, Cristian Muscas, Solomiya Pidkova, Mattia Bartoli, Massimo Rovere, and Alberto Tagliaferro. A comprehensive review on raman spectroscopy applications. *Chemosensors*, 9(9):262, 2021.

[30] Sanjay M Nilapwar, Maria Nardelli, Hans V Westerhoff, and Malkhey Verma. Absorption spectroscopy. In *Methods in enzymology*, volume 500, pages 59–75. Elsevier, 2011.

[31] Azad Mohammed and Avin Abdullah. Scanning electron microscopy (sem): A review. In *Proceedings of the 2018 international conference on hydraulics and pneumatics—HERVEX, Băile Govora, Romania*, volume 2018, pages 7–9, 2018.

[32] James Cook. The relationship between electrical energy and chemical energy. *Archives in Chemical Research*, 2022.

[33] James F Rusling and Steven L Suib. Characterizing materials with cyclic voltammetry. *Advanced Materials*, 6(12):922–930, 1994.

[34] Tanushree Ghosh, Love Bansal, Suchita Kandpal, Chanchal Rani, Deb Kumar Rath, Bhumika Sahu, Sandeep Chhoker, and Rajesh Kumar. Multifunctional electrochromic hybrid pani@ wo3 core-shell for energy generation and storage. *Journal of Energy Storage*, 72:108640, 2023.

[35] Muhammad Farhan Zainal, Yusairie Mohd, and Ruhani Ibrahim. Preparation and characterization of electrochromic polyaniline (pani) thin films. In *2013 IEEE Business Engineering and Industrial Applications Colloquium (BEIAC)*, pages 64–68. IEEE, 2013.

[36] Love Bansal, Bhumika Sahu, Deb Kumar Rath, Nikita Ahlawat, Tanushree Ghosh, Suchita Kandpal, and Rajesh Kumar. Stoichiometrically optimized electrochromic complex [v2o2+ ξ (oh) 3-ξ] based electrode: Prototype supercapacitor with multicolor indicator. *Small*, 20(32):2312215, 2024.

[37] Tej B Limbu, Basant Chitara, Jason D Orlando, Martha Y Garcia Cervantes, Shalini Kumari, Qi Li, Yongan Tang, and Fei Yan. Green synthesis of reduced ti 3 c 2 t x mxene nanosheets with enhanced conductivity, oxidation stability, and sers activity. *Journal of Materials Chemistry C*, 8(14):4722–4731, 2020.

[38] Bhumika Sahu, Mayank K Singh, Love Bansal, Deb Kumar Rath, Dhirendra K Rai, and Rajesh Kumar. Ti3c2tx-mxene-based color-indicative all-organic electrochromic supercapacitors. *Advanced Engineering Materials*, 26(23):2401295, 2024.

[39] Sheheera Irfan, Yasir A Haleem, Muhammad Usman, Naseeb Ahmad, Muhammad Arshad, Muhammad Imran Irshad, Muhammad Farooq Saleem, Muhammad Habib, Rashid Khan, and Serdar Altin. Validating superior electrochemical properties of ti 3 c 2 mxene for supercapacitor applications through first-principles calculations. *New Journal of Chemistry*, 48(11):4982–4994, 2024.

[40] Tanushree Ghosh, Love Bansal, Suchita Kandpal, Chanchal Rani, Manushree Tanwar, and Rajesh Kumar. Ambipolar all-organic solid-state electrochromic device using electrodeposited polyaniline: improving performance by design. *ACS Applied Optical Materials*, 1(1):473–480, 2022.